# Magnetospheric Multiscale Mission

# Electron Drift Instrument

# Data Products Guide

UNH-MMS-EDIDPG-01
Revision 1.2
18 March 2016

Prepared by

MMS EDI Team

University of New Hampshire

Space Science Center

**Change record**

| Revision | Date | Author | Description / Modifications |
|---|---|---|---|
| Draft 1.0 | March 1, 2013 | Chutter | Initial Draft |
| Draft 1.1 | May 2, 2013 | Chutter | Revised Draft |
| 1.2 | March 18, 2016 | Vaith | First Release |

**Table of Contents**

# 1 Introduction

## 1.1 Scope

This Data Products Guide for the Electron Drift Instrument (EDI) of NASA's Magnetospheric Multiscale Mission (MMS) contains the description and specification of the Level 2 data products generated by the MMS Science Data Center (SDC) in collaboration with the EDI instrument team. The EDI team is responsible for the development and maintenance of the data processing software to produce all EDI data products. Data processing is run at the SDC and at UNH.

## 1.2 Abbreviations

AFG..... Analog Flux Gate Magnetometer
AHBROM..... Advanced High Performance Bus Read Only Memory
CDF..... Common Data Format
CEB..... FIELDS Central Electronics Box
CRAM..... Chalcogenide Random Access Memory (non-volatile)
DFG..... Digital Flux Gate Magnetometer
DSL..... Despun Angular Momentum (coordinate system)
EDAC..... Error Detection and Correction
EDI..... Electron Drift Instrument
FIELDS..... MMS instrument suite for measuring fields and waves
FPGA..... Field Programmable Gate Array
FWHM..... Full width at half maximum
GDE..... Gun-Detector Electronics
GDU..... Gun-Detector Unit
GSE..... Geocentric Solar Ecliptic (coordinate system)
GSM..... Geocentric Solar Magnetospheric (coordinate system)
J2000..... Standard Epoch equivalent to 2000-01-01T11:58:55.816 UTC
MCP..... Micro-Channel Plate
MMS..... Magnetospheric Multiscale Mission
SDC..... Science Data Center
SNR..... Signal-to-Noise Ratio
SRAM..... Static Random Access Memory
TOF..... Time-of-Flight
TT2000..... Time tag format for representation of absolute times in nanoseconds since J2000
UNH..... University of New Hampshire

## 1.3 Documents

| Title | Issue | Date |
|---|---|---|
| MMS SDC Developer Guide | 1.9 | 04/11/2014 |
| MMS CDF Format Guide | 1.8 | 01/19/2016 |
| MMS EDI Instrument User Manual | Rev 1 | 03/27/2013 |
| CDF User's Guide | 3.6 | 02/20/2015 |
| MMS Alignment and Coordinate Systems Document | Rev C | 07/22/2014 |

# 2 Instrument Description

## 2.1 Functional Principle

The Electron Drift Instrument measures the electron drift velocity, $\mathbf{V_d}$ , by detecting the displacement of two weak beams of test electrons, launched from two electron guns located on opposite sides of the spacecraft. The technique intrinsically measures both components of the drift in the plane perpendicular to the ambient magnetic field, **B**, for arbitrary orientations of $\mathbf{V_d}$ and **B** with respect to the spacecraft spin axis. The physical basis of the measurement is the perturbation of the electron's gyro orbit from the circular trajectory that it would follow in the absence of a drift. This perturbation can be measured in two different ways in order to determine the magnitude and direction of the electron drift velocity. The first method uses the fact that the perturbed trajectory of an electron beam, fired perpendicular to the ambient magnetic field, returns to the spacecraft after one or more gyro orbits only when fired in unique directions (see Figure 1). By finding these directions, one can deduce the drift velocity using a "triangulation" technique.

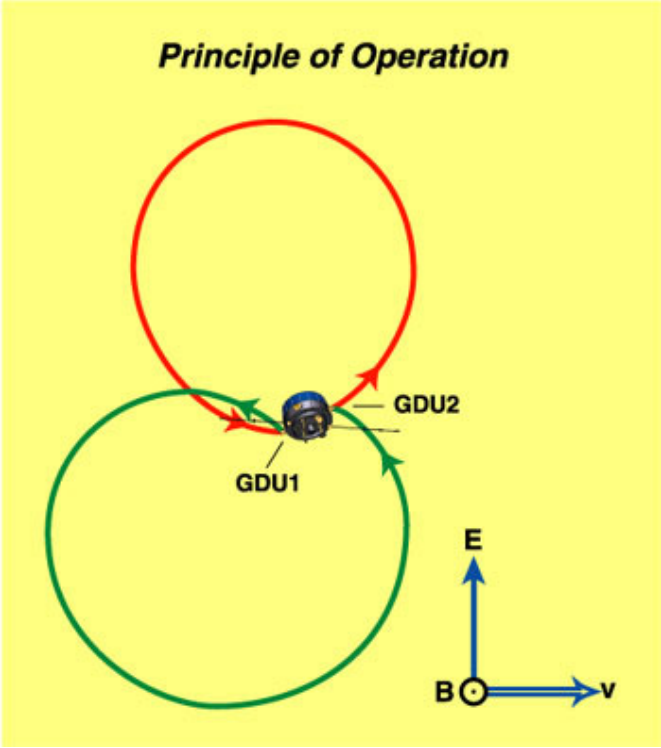


Figure 1: EDI functional principle

The second method measures the times-of-flight (TOF) for the electron beams to return to the spacecraft, which in the presence of a drift, differ from the gyro period by amounts that are proportional to $\pm\mathbf{V_d}$ . The two techniques are complementary in that triangulation is most accurate for small-to-moderate drifts, while the time-of-flight is better for moderate-to-large drifts. The electric field is derived from the measured drift velocity by assuming that the drift is solely due to an electric field. As a by-product of the TOF measurement, the magnitude of the magnetic field can be determined with high accuracy and thus EDI can help in the determination of offsets in the flux gate magnetometer sensors of AFG and DFG.

The Electron Drift Instrument can also be used as a particle detector that allows sampling of ambient plasma electrons at selected pitch angles with high time resolution.

## 2.2 Hardware Overview

The Electron Drift Instrument consists of two identical Gun-Detector Units (GDU) that are mounted on opposite sides of the spacecraft (cf. Figure 2) and a Controller that is implemented on an electronics board inside the FIELDS Central Electronics Box (CEB). The Controller and the GDUs exchange information via a serial command/data interface. Inside the CEB the EDI Controller interfaces with the FIELDS Central Data Processing Unit (CDPU) from which it receives commands and timing information and to which it sends telemetry. See Figure 2 for a top level block diagram.

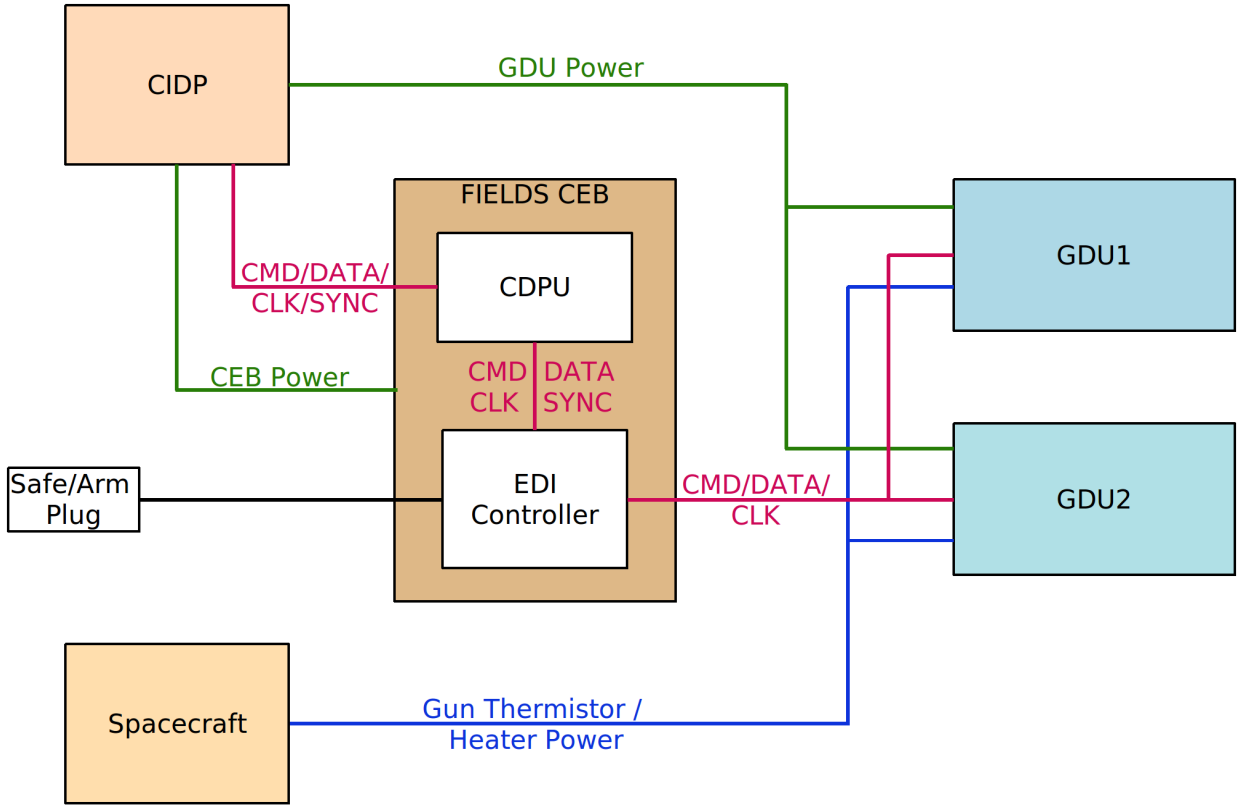


Figure 2: EDI top level block diagram

### 2.2.1 EDI Controller

The core of the EDI Controller is an ACTEL RTAX2000 FPGA with the following components:

- Fault tolerant LEON3, including EDAC for external memory (non-volatile RAM, SRAM) and AHBROM that contains the BOOT/FAILSAFE code.
- Interfaces to the CDPU and to the GDUs, including EDAC for the respective interface memories
- Watchdog

External to the FPGA, the EDI Controller has 2 MBytes of non-volatile RAM (CRAM) and 2 MBytes of SRAM.

### 2.2.2 Gun-Detector Unit

Each GDU consists of a gun, a detector and a gun-detector electronics box (GDE). The detector is subdivided into an electrostatic optics and a Sensor (see Figure 3).

The gun hosts a beam generation system, high voltage supply, 13 high voltage amplifiers and a deflection head consisting of eight deflection electrodes which, together with a delicate retarding grid, allow the deflection of a narrow electron beam into any direction over slightly more than one hemisphere.

A total of nine optics electrodes is used to focus and guide the returning electron beam onto the annular micro-channel plate (MCP) in the sensor. The voltages on the upper five optics electrodes define the polar look angle, which is the center angle of the polar acceptance window (FWHM) with respect to the instrument symmetry axis (horizontal in Figure 3) from which the optics accepts electrons. The polar angle can be anywhere between 0 degrees (looking along the instrument symmetry axis) and more than 100 degrees. The optics is capable of handling even slightly negative look angles. This feature is, however, not required for successful operation. The design of the optics allows, for a given look angle, the selection of one of several optics states, which differ in polar FWHM, geometric factor, and sensitivity to a mono-directional, mono-energetic return beam. The optics state is chosen by the flight software or by command to give the best results in a given plasma environment. The lower four optics electrodes depend only on beam energy, but not on the optics look angle. They consist of an electrostatic analyzer, and two additional electrodes (not shown in Figure 3) located between the analyzer and the MCP to allow radial adjustment of the positions where the electrons impinge on the MCP input surface.

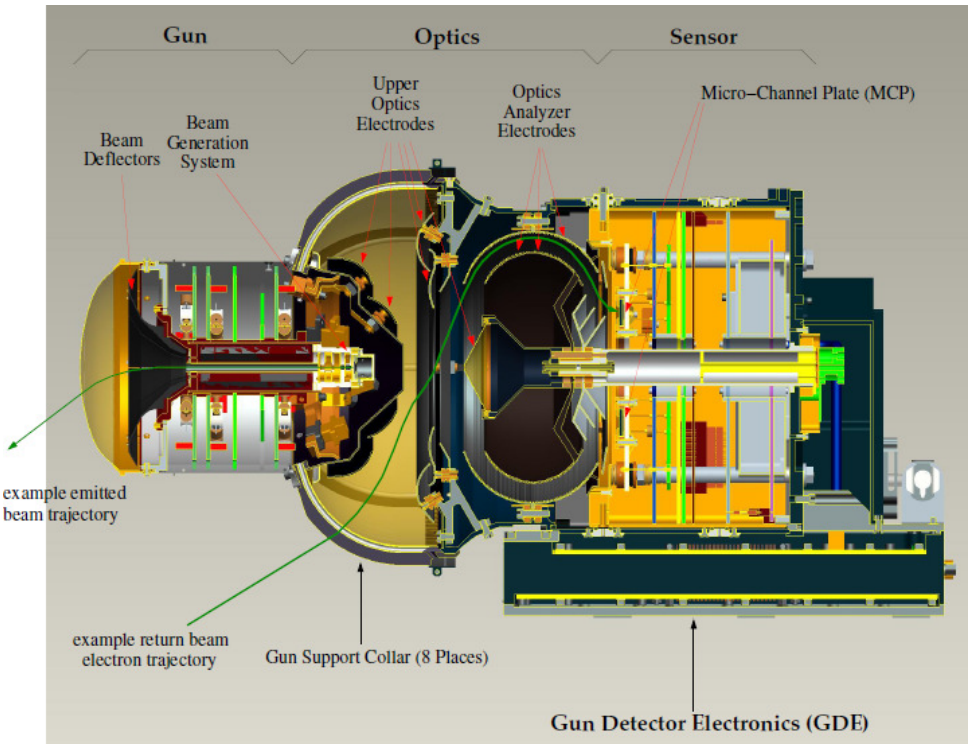


Figure 3: Cross-sectional view of a Gun-Detector Unit

The sensor divides the annular area below the MCP into 32 azimuthal sectors of 11.25 degrees each, with 32 corresponding pre-amplifiers, out of which four arbitrarily selectable channels can be transmitted to the GDE, where events are further processed.

The GDE contains an Actel FPGA (called FPGA1) that interfaces to the Controller in the CEB via a serial command/data interface. Four 16-bit accumulators count event pulses received from the sensor. Any two of these four channels may be selected and merged. The combined signal is sent to a second FPGA (called FPGA2), a re-programmable Xilinx FPGA) in which the TOF correlator is implemented. The GDE also generates reference voltages for both gun and optics high voltages, and has a high voltage stack as well as high voltage amplifiers for seven of the nine optics electrodes.

The gun has its own high voltage stacks for the beam generation system and the deflection head, and supplies also the high voltages for the upper two optics electrodes. The sensor has its own high voltage power supply for the MCP module. High voltage outputs are in the range -1kV to +3.5 kV. The high voltage stacks in GDE, gun and sensor can be switched on separately. In addition to the high voltage supply switches there is a separate switch to control the supply of the cathode of the electron beam generation system.

An electronic block diagram of a GDU is shown in Figure 4.

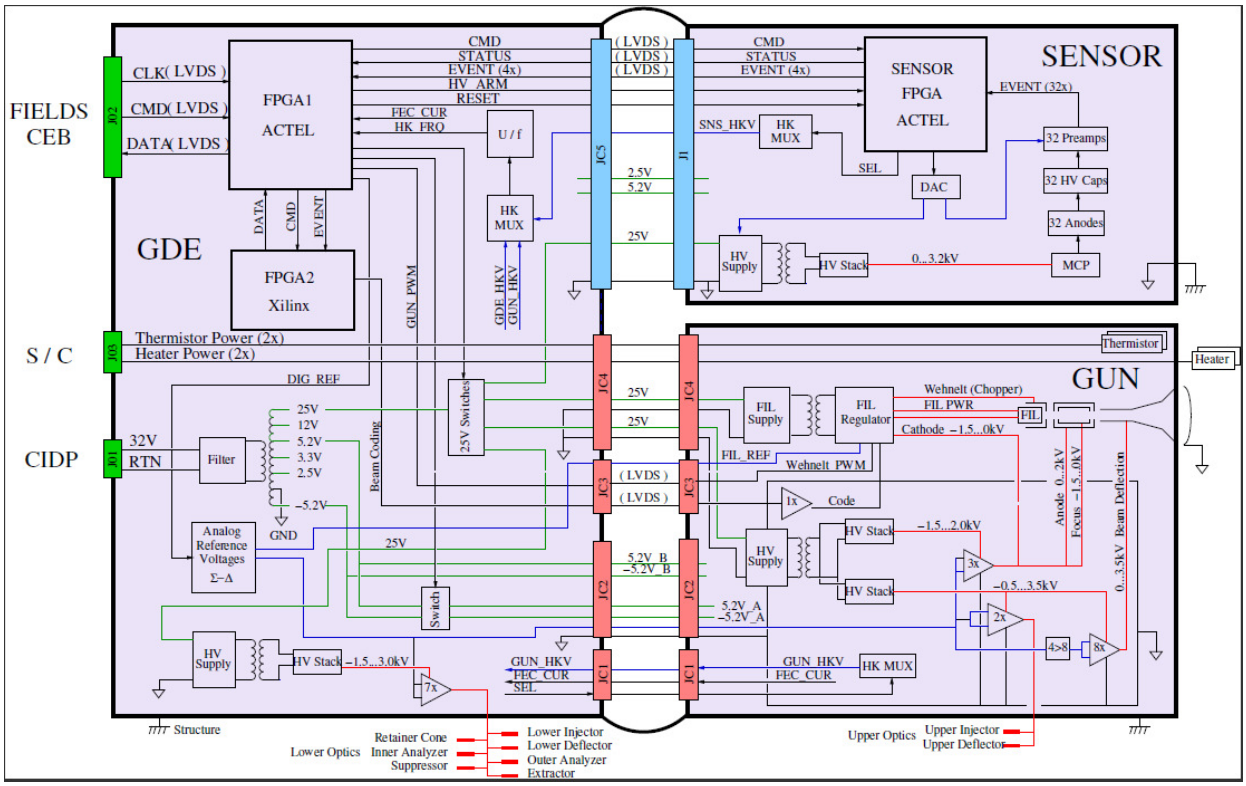


Figure 4: Electronic block diagram of a Gun-Detector Unit

## 2.3 EDI Operation

EDI has two scientific data acquisition modes, called electric field mode and ambient mode. In electric field mode two coded electron beams are emitted such that they return to the detectors after one or more gyrations in the ambient magnetic and electric field. The firing directions and times-of-flight allow the derivation of the drift velocity and electric field. In ambient mode the electron beams are not used. The detectors with their large geometric factors and their ability to adjust the field of view quickly allow continuous sampling of ambient electrons at a selected pitch angle and fixed but selectable energy.

### 2.3.1 Electric Field Mode Operation

To find the beam directions that will hit the detector, EDI sweeps each beam in the plane perpendicular to **B** at a fixed angular rate of 0.22°/ms until a signal has been acquired by the detector. Once signal has been acquired, the beams are swept back and forth to stay on target. Beam detection is not determined from the

changes in the count-rates directly, but from the square of the beam counts divided by the background counts from ambient electrons, i.e., from the square of the instantaneous signal-to-noise-ratio, $SNR^2$. This quantity is computed from data provided by the correlator in the Gun-Detector Electronics that also generates the coding pattern imposed on the outgoing beams. If the squared signal-to-noise ratio exceeds a threshold, this is taken as evidence that the beam is returning to the detector. The thresholds for $SNR^2$ are chosen dependent on background fluxes. They represent a compromise between getting false hits (induced by strong variations in background electron fluxes) and missing true beam hits. The basic software loop that controls EDI operations is executed every 2 ms. As the times when the beams hit their detectors are neither synchronized with the telemetry nor equidistant, EDI data have no fixed time-resolution. Data are reported in telemetry slots. In Survey, using the standard packing mode 0, there are eight telemetry slots per second and GDU. The last beam detected during the previous slot will be reported in the current slot. If no beam has been detected the data quality will be set to zero. In Burst telemetry there are 128 slots per second and GDU. The data in each slot consists of information regarding the beam firing directions (stored in the form of analytic gun deflection voltages), times-of-flight (if successfully measured), quality indicators, time stamps of the beam hits, and some auxiliary correlator-related information.

### 2.3.2 Ambient Electron Mode Operation

#### *2.3.2.1 Basic Operation*

Whenever EDI is not in electron drift mode it uses its ambient electron mode. The mode has the capability to sample at either 90 degrees pitch angle or at 0/180 degrees (field aligned), or to alternate between 90 degrees and field aligned with selectable dwell times. While all options have been demonstrated during the commissioning phase, only the field aligned mode has been used in the routine operations phase. The choices for energy are 250eV, 500eV and 1keV. The two detectors, which are facing opposite hemispheres, are looking strictly into opposite directions, so while one detector is looking along **B** the other is looking antiparallel to **B** (corresponding to pitch angles of 180 and 0 degrees, respectively). The two detectors switch roles every half spin of the spacecraft as the tip of the magnetic field vector spins outside the field of view of one detector and into the field of view of the other detector.

#### *2.3.2.2 Sensor Anode Selection*

The EDI detector allows the selection of four arbitrary (out of 32) sensor anodes. In practise, however, the flight software always selects four adjacent anodes. The selection is governed by the magnetic field orientation with respect to the GDU instrument axes such that the anodes will pick up those electrons that are entering the detector from directions close to **B** (or antiparallel to **B**). Two different algorithms have been used for the detailed placement of the four adjacent anodes with respect to **B**:

- **amb** -- Up until January 4, 2016 the anodes were chosen such that the magnetic field vector projected into the plane of the micro-channel plate entry surface was best aligned with the center of the four anodes ( that is, with the gap between the inner two of the four anodes). Data taken in this configuration are using the term “amb” in the data product names. In the burst data where four channels (corresponding to the four adjacent sensor anode pads) are sampled per GDU, the average (or sum) of the center two channels (channels 2 and 3) represents best the pitch angle of 0 degrees (or 180 degrees).
- **amb-pm2** -- Starting January 4, 2016, the anodes were chosen such that the projection of the magnetic field vector was best aligned with the center of the first (that is, outer) of the four anodes. This provides coverage of a larger range of pitch angles in general. Data taken in this configuration are identified by the term “amb-pm2” in the data product names. In the burst data where four channels (corresponding to the four adjacent sensor anode pads) are sampled per GDU, channel 1 represents best the pitch angle of 0 degrees (or 180 degrees).

#### 2.3.2.3 Telemetry

In survey telemetry there are 32 counts samples per detector and per second. Each sample is accumulated over 15.625 ms (1/64 seconds), which means that the sampling is not contiguous. In the "amb" configuration (see section 2.3.2.2) the two center anodes of the four selected anodes are summed up and reported as a single number for each of the 32 samples per second. In the "amb-pm2" configuration only counts from the outer anode that is best aligned with **B** are reported. In addition to the counts data, GDU1 detector look directions are reported, as well a flag that indicates the pitch angle for the detector in GDU1. Since the two detectors are looking antiparallel to each other at all times this is sufficient to determine the look direction and pitch angle for the other detector as well. It is noted that the directions and pitch angle flags reported in telemetry represent the situation in the center of the accumulation window for each sample. A second flag ("contamination flag") indicates if a switch from 0 to 180 degrees pitch angle occurred while the detector was accumulating data.

In Burst telemetry there are 1024 counts samples per detector and per second, and the accumulation time is approximately 1ms (1/1024 seconds), so the sampling is contiguous. The counts data are reported separately for each of the four anodes. They are compressed using a lossy quasi-logarithmic 12-to-8 bit compression. As in the case of survey telemetry there are directions (angles) and flags reported in addition to the counts data. The reporting rate for angles is 128 per second. Flags are reported at a rate of 512 per second.

# 3 Data Processing

## 3.1 Overview

The following Level 2 and Quicklook EDI data products are being generated.

- **Electric Field Data** ("l2_efield") -- This is the primary data product generated from data collected in electric field mode. The science data generated are drift velocity and electric field data in various coordinate systems. They are derived from triangulation and/or time-of-flight analysis. Where both methods are applicable, their results will be combined using a weighting approach based on their relative errors.
- **Quality-Zero Data** ("l2_q0") -- These data are a by-product generated from data collected in electric field mode. Whenever no return beam is found in a particular time slot by the flight software, the data to be reported will be flagged with the lowest quality level (quality zero). The ground processing generates a separate data product from these counts data.
- **Ambient Electron Data** ("l2_amb", "l2_amb-pm2") -- The raw counts data collected in ambient mode are going through a two step calibration for conversion to fluxes. The first step performs a dead time correction of the raw counts and applies a relative calibration that removes the instrument response dependency on look direction (optics polar angle and sensor anode pad number). The second step is a multiplication with a factor to convert from relative, dead time corrected counts to fluxes.
- **Ambient Electron Quicklook Data** ("ql-amb", "ql-amb-pm2") -- The quicklook data are corrected for dead time and instrument response function, but - unlike the L2 ambient electron data - lack the absolute calibration.
- **Ambient Electron Calibration Data** ("cal_l2_amb") -- This data product contains the relative and absolute calibration data necessary for the conversion of the raw counts collected in ambient mode to fluxes.

## 3.2 Electric Field Mode Data Processing

Generation of L2 Electric Field Mode data is a three step process as illustrated in Figure 5. In the first step L1A files are generated from L0 raw telemetry. Aside from extraction of data this involves a conversion of the analytic voltages that represent the gun firing direction in the L0 data to the azimuth and polar angles of a spherical coordinate system that has its Z axis along the GDU symmetry axis pointing outward in the

spacecraft spin plane and the X axis along the negative spacecraft body Z axis. In addition, since the return beam hits are asynchronous in nature to any onboard clock, separate time tags in TT2000 format are calculated for every individual beam based on the timing information in the L0 files. Raw times-of-flight in digital units are converted to micro-seconds.

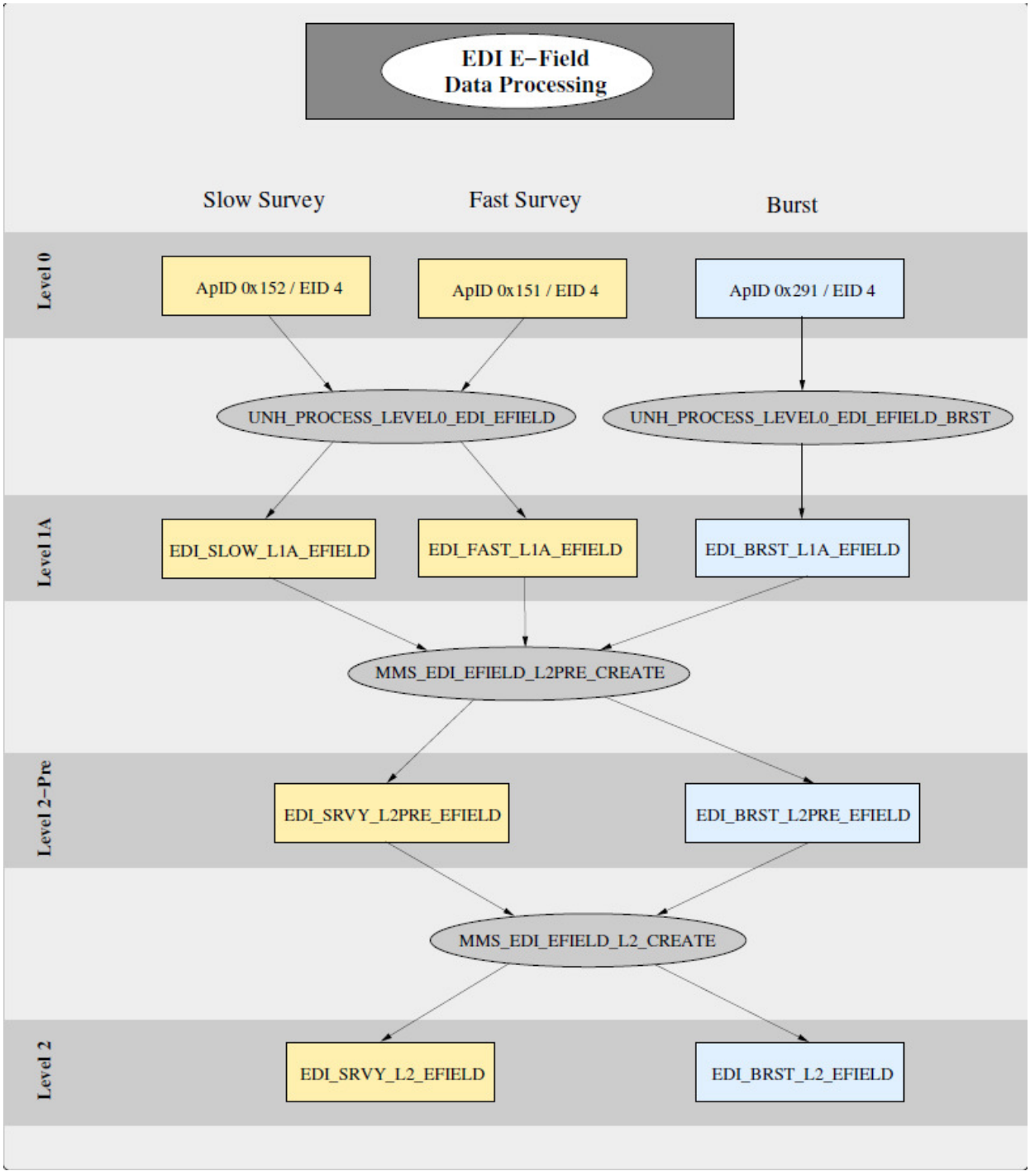


Figure 5: EDI Electric Field Mode Data Processing Flow

In the second step the L1A data are processed to level L2-Pre. Data are preselected by quality and are sent through a process that attempts to determine the number of gyrations for each beam based on its time-of-

flight and the gyro time derived from DFG L2Pre magnetic field data. The resulting data set is analyzed with both the triangulation and time of flight method as outlined further below. For the purpose of the analysis the data are grouped into five-second time intervals. For each analysis interval an average magnetic field vector is calculated for the definition of a gyro plane, that is, the plane perpendicular to the magnetic field. Beam firing directions are then represented as clock angles in that plane with respect to a reference direction which is chosen to be closest to the line towards the sun.

### 3.2.1 Triangulation Analysis

The triangulation analysis procedure determines the drift step by searching for the target-point that minimizes an appropriate 'cost-function'. The cost-function is constructed, for each grid-point in the plane, by adding up the (squared) angle-deviations of all beams in a chosen time interval from the direction to that grid-point. Each beam contribution to the cost-function is normalized by the (squared) error in the firing directions, which is a function of beam pointing direction and varies between 1° and 4°, using an analytic model for the beam profile as a function of the polar angle of the gun firing direction. The grid-point with the smallest value of the cost-function is taken as the target. If a beam has been identified as a multi-runner of order *N* by the preceding runner order analysis, it is associated with a grid-point at *N* times the radial distance. When identification of the order from the runner order analysis is ambiguous, the respective beams are treated as single-runners. This assumption works well in most cases, as, compared the EDI implementation on ESA's Cluster project, the design of the correlator and the choice of code frequencies makes the occurrence of multi-runners much less likely. To speed up the search, the procedure uses a coarse grid to identify a restricted range in which the final search is performed with a much finer grid. The electron trajectories are approximated by circles whose radius is based on the magnetic field strength.

The analysis fails if the drift step and/or the magnetic field significantly vary within the chosen time interval (5 seconds). Such cases can be identified by the variance in the magnetic field, by the quality of the fit (as measured by its reduced $\chi^2$), and by the errors in the computed drift step.

Using the DFG L2pre magnetic field data, the drift steps can be converted to drift velocities and electric field data.

Errors are determined from the radial and azimuthal extent of the 95% confidence level iso-contour of the 2-dimensional cost function, and are propagated from the 2-dimensional drift step in the gyro-plane to the 3-dimensional drift velocity and electric field vectors in the target coordinate systems.

In addition to the drift step, drift velocity and electric field vectors and their respective errors, various processing parameters such as the number of beams involved in the analysis and the reduced $\chi^2$ are stored in the resulting L2pre data files for the purpose of reducing the L2pre data set to L2 data as described in section 3.2.3.

### 3.2.2 Time-of-Flight Analysis

Deduction of the drift step (and the drift velocity) from analysis of the difference in the times-of-flight of the two beams is, in principle, straightforward. If the drift step is large enough such that the firing directions become nearly parallel, the beams in the analysis interval can be grouped into two nearly oppositely directed sets. The set with the larger times-of-flight then must contain the beams directed towards the target, the other set those directed away from the target. This assignment settles the drift direction, and the drift magnitude is then computed from the magnitude of the difference in the times-of-flight.

This simple scheme would require stable conditions (i.e., non-varying gyro time and times-of-flight) over the analysis interval. Since this is not always the case, especially in the magnetosheath, the analysis makes use of the gyro time determined from the DFG L2pre data and interpolated to the times of the EDI beam hits. The differences between the measured times-of-flight and the interpolated gyro times are calculated separately for the two sets of beams. For each set the average difference from the gyro time is calculated and the two

averages are then combined. This way any fixed magnitude offset in the gyro-time that might result from a residual error in the magnetic field calibration will cancel out. The set with the larger average identifies the direction towards the target. Multiplication of half the time-of-flight difference (the combination of the two averages as described above) with the electron velocity yields the drift step magnitude.

Calculation of drift velocities and electric fields is done in the same fashion as for the triangulation analysis.

The error on the drift step magnitude is computed using the Student's t-test which measures the significance of a difference of means. The error is reported at the 95% confidence level. The azimuthal error is determined from the spread of the firing directions. Propagation of the errors to the 3-dimensional drift velocity and electric field vectors is done in the same way as for the triangulation analysis.

### 3.2.3 Filtering of L2Pre Data

In the final step the L2Pre data are filtered using various quantities stored in the L2pre files. For triangulation, the filter criteria are:

- Reduced $\chi^2$ below 1000
- At least three beams in the analysis interval
- Beam spread is less than 15 degrees
- Drift step magnitude is less than 3 times the triangulation baseline
- Electric Field error is less than 1 mV/m
- Electric Field error is larger than 0.1 mV/m
- The relative error of the electric field magnitude less than 1 (100%)

For the time-of-flight analysis the filter criteria are:

- Drift step magnitude greater than 1 meter
- Electric field error less than 1 mV/m
- Relative error of electric field magnitude less than 1 (100%)

## 3.3 Quality Zero Data Processing

The lowest quality level in the raw (and in the L1A) electric field data (quality zero) signals that no return beam was detected during a given time slot. Counts accumulated in these time slot are considered a proxy for the ambient electron flux at the energy of the detector. In regions with high variability of the magnetic/electric fields, very low magnetic fields, or high ambient electron fluxes at the energy of the detector, EDI will have difficulty identifying the return beams (if there are any). Consequently, in those regions there will be a higher rate of quality-zero data. Care must be taken in general when interpreting these data. First, they are uncalibrated raw counts. Second, even though they did not pass the detection threshold for the squared signal-to-noise ratio, some of the counts samples can represent a mix of beam and background electrons. The data can be useful as boundary markers, or for detecting anisotropies in the 90 degree pitch angle data.

The processing extracts the counts data (one ms accumulation time base) and the gun firing directions. From the latter the associated detector look directions are deduced and the particle motion directions are calculated. Particle motion directions are specified in the form of azimuth and polar angle in the respective coordinate system (GSE, GSM) using the following convention:

- Polar angle = acos( z / magnitude )
- Azimuth angle = atan( y / x )

Since the counts are unmodified raw counts, no error is specified as it is straightforward for the user to calculate the one-sigma error (square root of the counts). The uncertainty in the particle motion direction is given as a single constant angular error number that is derived from the characteristic FWHM of the optics' polar acceptance and the half width of the sensor's azimuthal field of view.

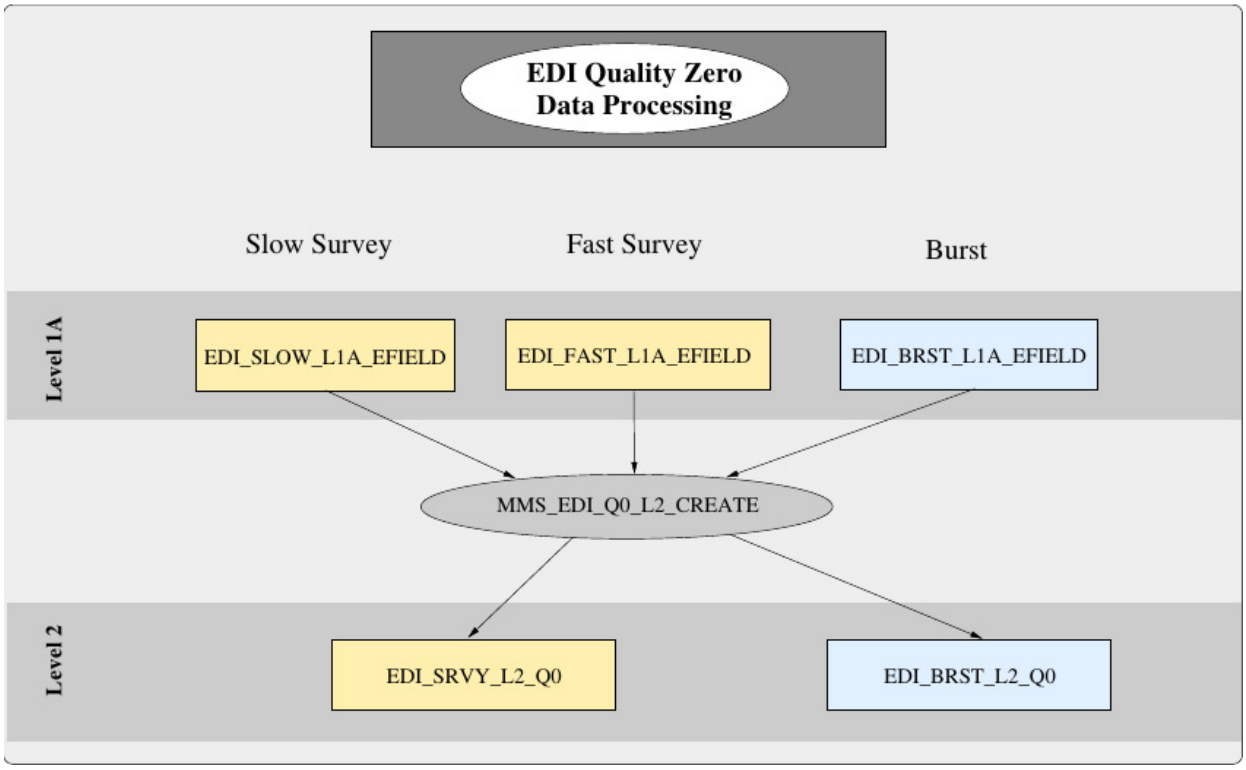


Figure 6: EDI Quality-Zero Data Processing

## 3.4 Ambient Electron Mode Data Processing

Ambient Mode data processing of Level 2 data and Quicklook (QL) data is illustrated in Figure 7. The initial common step is the generation of L1A data from the raw L0 data. In this step data are extracted, time tags in TT2000 format are added to each record, and for burst data the compressed counts data are decompressed.

For the QuickLook Data, the counts data are corrected for dead time effects and the instrument response function that removes the geometric factor dependency on the look direction is applied.

For the L2 ambient data, the absolute calibration factor is applied in addition, and an error for the resulting fluxes is calculated that takes into account various error terms as outlined in section 3.4.1. Particle motion directions are calculated and given in GSE and GSM coordinates. As in the case of the quality zero data the uncertainty in these directions is specified as a single angle.

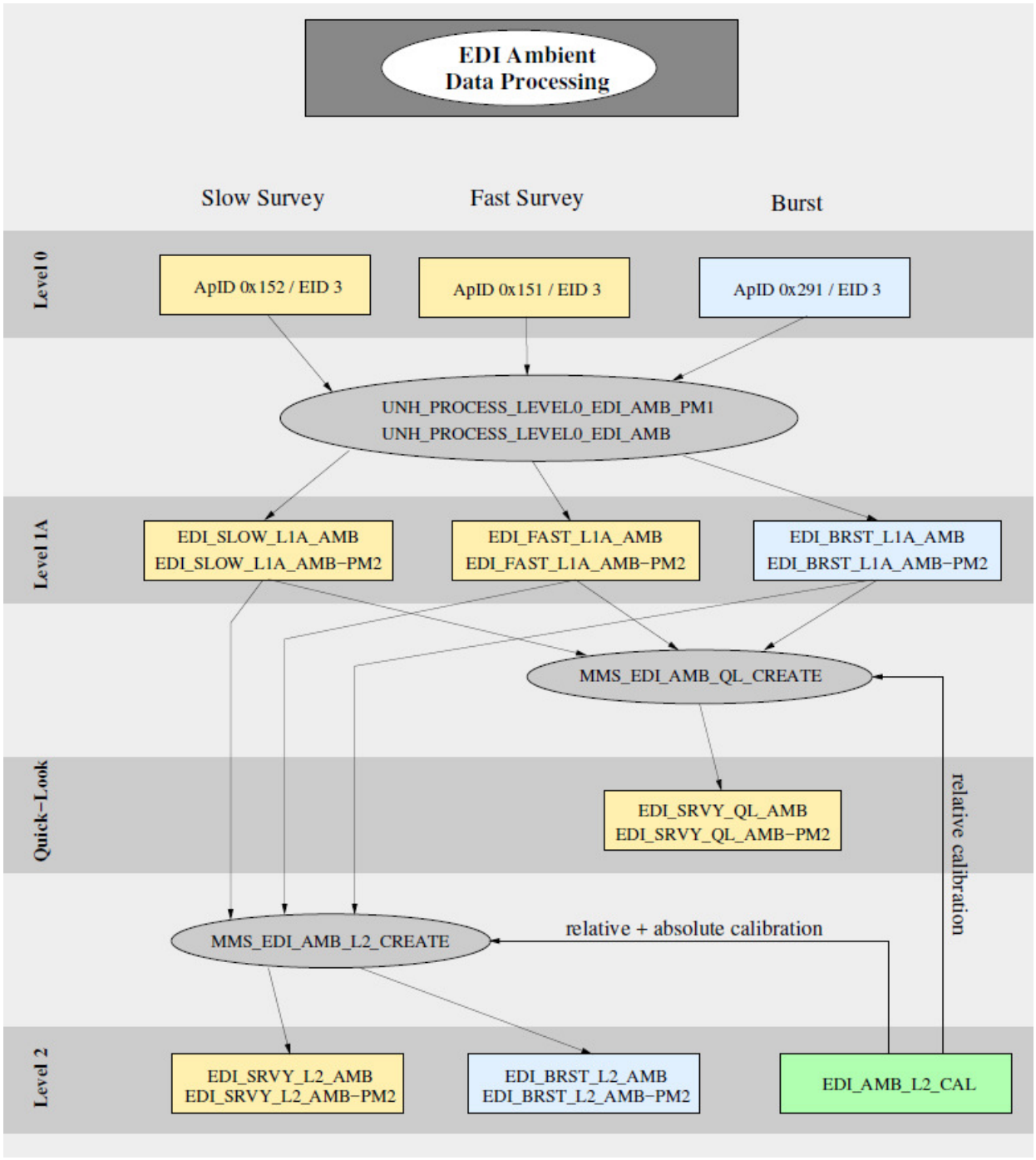


Figure 7: EDI Level 2 Ambient and Quicklook Ambient Data Processing Flow

### 3.4.1 Dead time correction

The dead time correction is given by

$$C = R \cdot t_A \; / \; ( \; t_A - R \cdot t_D )$$

with the following abbreviations:

| | |
|---|---|
| $C$ | dead time corrected counts |
| $R$ | raw counts |
| $t_A$ | the accumulation time (1/1024 sec for burst, 1/64 sec for survey) |
| $t_D$ | the sensor dead time (200ns) |

The error propagation from raw to dead time corrected counts is

$$err_C = err_R \cdot [ \, t_A \; / \; ( \; t_A - R \cdot t_D ) \, ]^2$$

where the one-sigma error *sqrt(R)* is used for $err_R$.

### 3.4.2 Calculation of ambient electron flux errors

The calculation of absolute fluxes is given by the formula

$$F = C \cdot R \cdot A$$

where

| | |
|---|---|
| $F$ | is the absolute flux |
| $C$ | is the dead time corrected counts |
| $R$ | is the relative calibration (a function of detector look angles) |
| $A$ | is the absolute calibration factor |

The error in the absolute flux is calculated according to

$$err_F = F \cdot \; SQRT \, [ \; (err_C / C)^2 + (err_R / R)^2 + (err_A / A)^2 \; ]$$

The error $err_C$ for the dead time corrected counts is given in section 3.4.1. The second term $err_R/R$ is ignored at the moment, as the information on the relative calibration is still being improved, especially for small polar look angles where the relative calibration $R$ factor is largest. For the third term $err_A/A$, we assume a factor of 0.2 (20% error), based on the general level of agreement in comparisons between DES burst quicklook data and EDI ambient burst data.

## 3.5 Ambient Electron Data Calibration Process

Two kinds of calibrations are stored in the EDI L2 ambient calibration data. The first is the relative calibration that describes the instrument response function. It is used to remove instrumental effects such as geometric factor dependence on look angle as best as possible. This calibration is done with L1A EDI burst ambient data from selected quiet regions where the assumption of time invariance of ambient fluxes is made to derive the instrument response function.

The second calibration (absolute calibration) makes use of selected DES Quicklook data in the energy band closest to the EDI detector energy and in pitch angle bins 0 and 180 in order to derive a factor that, when applied to the dead time corrected and relative calibrated EDI data, provides an overall agreement between EDI and DES.

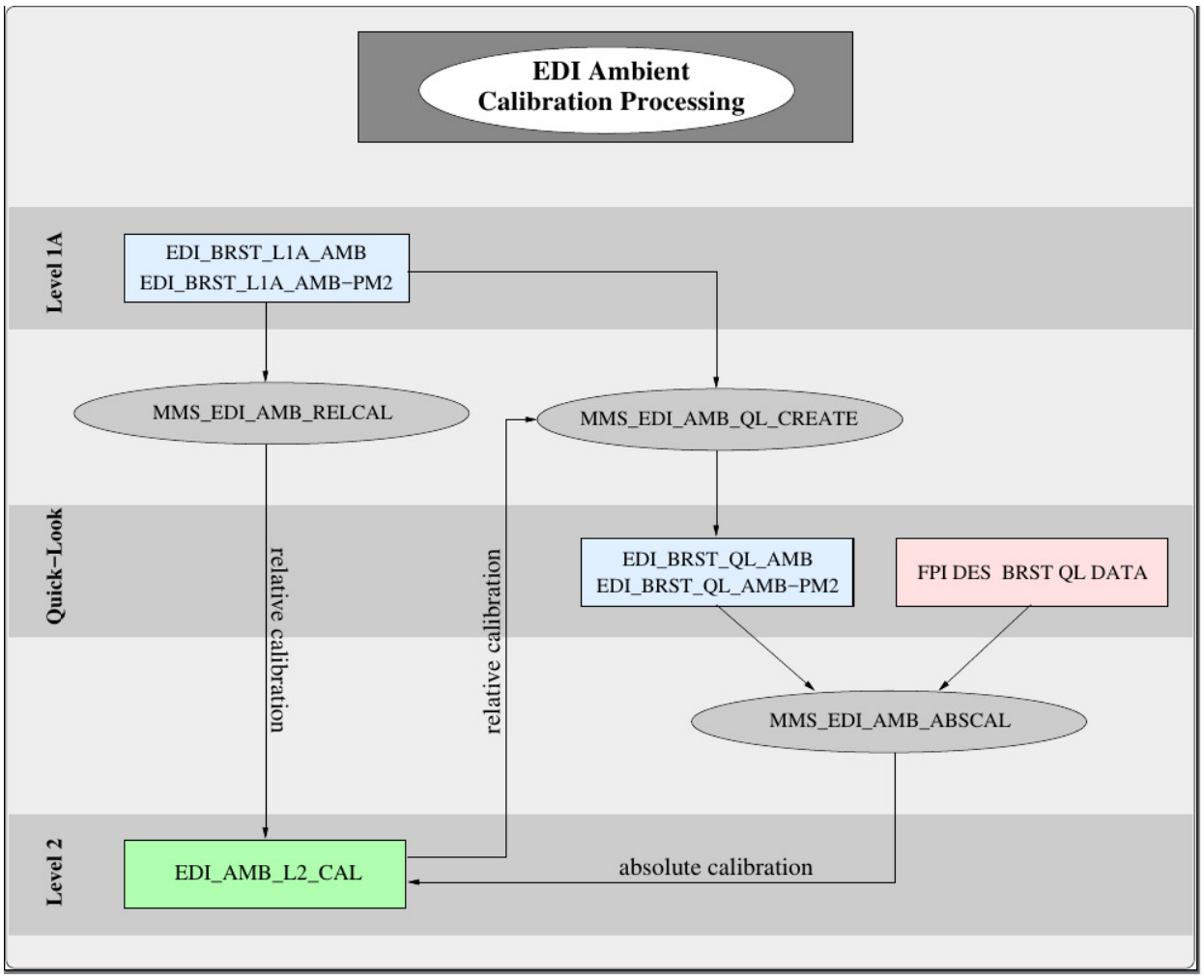


Figure 8: Generation of EDI Ambient Electron Calibration Data

# 4 Level 2 Data Products

This section provides listings of the variables in each of the EDI L2 data products:

- EDI L2 Electric Field Data
- EDI L2 Quality Zero Data
- EDI L2 Ambient Mode Data
- EDI L2 Ambient Mode Calibration Data

In the file and variable names given in the subsequent sections the following generic tags are used

| | |
|---|---|
| <N> | Observatory number (actual values are 1,2,3,4) |
| <tlm> | Telemetry identifier (srvy for Survey, brst for Burst) |
| <yyyymmdd> | Year (yyyy), month (mm) and day (dd) |
| <yyyymmddhhmmss> | Year, month, day (as above), hour (hh), minute (mm) and second (ss) |
| <x.y.z> | CDF file version identifier |

In the ambient mode and quality-zero data products, trajectories of observed particles are given as 2-dimensional quantities, containing the azimuth and polar angles of the directions in the first and second component, respectively, for the specified coordinate system. The angles follow the standard definition of spherical polar coordinate systems in physics. The azimuth angle defines the projection of the motion vector into the XY plane. It is zero along +X and 90 degrees along +Y. The polar angle is counted with respect to the Z axis of the particular coordinate system.

## 4.1 Electric Field Data

For the L2 electric field data product, survey and burst files contain the same quantities with only the telemetry identifier (<tlm>) being different (<tlm> = srvy or <tlm> = brst).

Filenames:

mms<N>_edi_srvy_l2_efield_<yyyymmdd>_v<x.y.z>.cdf
mms<N>_edi_brst_l2_efield_<yyyymmddhhmmss>_v<x.y.z>.cdf

| Name | Description | Type | Unit |
|---|---|---|---|
| mms<N>_edi_vdrift_dsl_<tlm>_l2 | Drift velocity vector in DSL coordinates | FLOAT | km/s |
| mms<N>_edi_vdrift_gse_<tlm>_l2 | Drift velocity vector in GSE coordinates | FLOAT | km/s |
| mms<N>_edi_vdrift_gsm_<tlm>_l2 | Drift velocity vector in GSM coordinates | FLOAT | km/s |
| mms<N>_edi_e_dsl_<tlm>_l2 | Electric field vector in DSL coordinates | FLOAT | mV/m |
| mms<N>_edi_e_gse_<tlm>_l2 | Electric field vector in GSE coordinates | FLOAT | mV/m |
| mms<N>_edi_e_gsm_<tlm>_l2 | Electric field vector in GSM coordinates | FLOAT | mV/m |
| mms<N>_edi_tri_weight_<tlm>_l2 | Weight of triangulation method when merging results from triangulation and time-of-flight analyses | INT2 | percent |

| **Support Variables** | | | |
|---|---|---|---|
| Epoch | Time tags | TT2000 | ns since J2000 |
| mms<N>_edi_t_delta_minus_<tlm>_l2 | Time between start of analysis interval and time tag | INT8 | ns |
| mms<N>_edi_t_delta_plus_<tlm>_l2 | Time between time tag and end of analysis interval | INT8 | ns |
| mms<N>_edi_tri_rchisq_<tlm>_l2 | Reduced Chi-Squared from triangulation analysis | FLOAT | none |
| mms<N>_edi_v_dsl_delta_minus_<tlm>_l2 | Drift velocity negative error | FLOAT | km/s |
| mms<N>_edi_v_dsl_delta_plus_<tlm>_l2 | Drift velocity positive error | FLOAT | km/s |
| mms<N>_edi_v_gse_delta_minus_<tlm>_l2 | Drift velocity negative error | FLOAT | km/s |
| mms<N>_edi_ v_gse_delta_plus_<tlm>_l2 | Drift velocity positive error | FLOAT | km/s |
| mms<N>_edi_v_gsm_dsl_delta_minus_<tlm>_l2 | Drift velocity negative error | FLOAT | km/s |
| mms<N>_edi_v_gsm_dsl_delta_plus_<tlm>_l2 | Drift velocity positive error | FLOAT | km/s |
| mms<N>_edi_e_dsl_delta_minus_<tlm>_l2 | E-field negative error | FLOAT | mV/m |
| mms<N>_edi_e_dsl_delta_plus_<tlm>_l2 | E-field positive error | FLOAT | mV/m |
| mms<N>_edi_e_gse_delta_minus_<tlm>_l2 | E-field negative error | FLOAT | mV/m |
| mms<N>_edi_ e_gse_delta_plus_<tlm>_l2 | E-field positive error | FLOAT | mV/m |
| mms<N>_edi_e_gsm_dsl_delta_minus_<tlm>_l2 | E-field negative error | FLOAT | mV/m |
| mms<N>_edi_e_gsm_dsl_delta_plus_<tlm>_l2 | E-field positive error | FLOAT | mV/m |

## 4.2 Quality Zero Data

For the L2 quality zero data product, survey and burst files contain the same quantities with only the telemetry identifier being different (<tlm> = srvy or <tlm> = brst)

Filenames

mms<N>_edi_srvy_q0_l2_<yyyymmdd>_v<x.y.z>.cdf
mms<N>_ edi_brst_q0_l2_<yyyymmddhhmmss>_v<x.y.z>.cdf

| **Name** | **Description** | **Type** | **Unit** |
|---|---|---|---|
| mms<N>_edi_counts_gdu1_<tlm>_l2 | Raw counts measured by the detector in GDU1; accumulation time is 1/1024 seconds | UINT2 | counts |
| mms<N>_edi_counts_gdu2_<tlm>_l2 | Raw counts measured by the detector in GDU2; accumulation time is 1/1024 seconds | UINT2 | counts |
| mms<N>_edi_traj_gse_gdu1_<tlm>_l2 | Direction of particle motion for GDU1 electrons in GSE | FLOAT | degrees |
| mms<N>_edi_traj_gse_gdu2_<tlm>_l2 | Direction of particle motion for GDU2 electrons in GSE | FLOAT | degrees |
| mms<N>_edi_traj_gsm_gdu1_<tlm>_l2 | Direction of particle motion for GDU1 electrons in GSM | FLOAT | degrees |
| mms<N>_edi_traj_gsm_gdu2_<tlm>_l2 | Direction of particle motion for GDU2 electrons in GSM | FLOAT | degrees |
| **Support Variables** | | | |

| | | | |
|---|---|---|---|
| Epoch | Unused | TT2000 | ns since J2000 |
| epoch_gdu1 | Time tags for GDU1 counts and trajectories | TT2000 | ns since J2000 |
| epoch_gdu2 | Time tags for GDU2 counts and trajectories | TT2000 | ns since J2000 |
| epoch_timetag | Time tags for optics state variable | TT2000 | ns since J2000 |
| mms<N>_edi_optics_state_<tlm> _l2 | Optics State | UINT2 | none |
| mms<N>_edi_energy_gdu1_<tlm>_l2 | GDU1 detector energy | UINT2 | eV |
| mms<N>_edi_energy_gdu2_<tlm>_l2 | GDU2 detector energy | UINT2 | eV |

## 4.3 Ambient Electron Data

See section 2.3.2.2 for how especially the burst flux channels correspond to pitch angles.

### 4.3.1 Survey

File Names:

mms<N>_edi_srvy_l2_amb_<yyyymmdd>_v<x.y.z>.cdf
mms<N>_edi_srvy_l2_amb-pm2_<yyyymmdd>_v<x.y.z>.cdf

| Name | Description | Type | Unit |
|---|---|---|---|
| mms<N>_edi_flux1_0_srvy_l2 | Electron flux along pitch angle 0 | FLOAT | $cm^{-2}\ s^{-1}$ |
| mms<N>_edi_flux1_180_srvy_l2 | Electron flux along pitch angle 180 | FLOAT | $cm^{-2}\ s^{-1}$ |
| mms<N>_edi_traj1_gse_0_srvy_l2 | Direction of particle motion for pitch angle 0 electrons in GSE, given as in spherical coordinates. First component: azimuth (in GSE xy plane), second component: polar angle (with respect to GSE z) | FLOAT | degrees |
| mms<N>_edi_traj1_gsm_0_srvy_l2 | Direction of particle motion for pitch angle 0 electrons in GSM | FLOAT | degrees |
| mms<N>_edi_traj1_gse_180_srvy_l2 | Direction of particle motion for pitch angle 180 electrons in GSE | FLOAT | degrees |
| mms<N>_edi_traj1_gsm_180_srvy_l2 | Direction of particle motion for pitch angle 180 electrons in GSM | FLOAT | Degrees |
| **Support variables** | | | |
| epoch_0 | Time tags for pitch angle 0 variables: fluxes, trajectories, GDU numbers and errors | TT_2000 | ns since J2000 |
| epoch_180 | Time tags for pitch angle 180 variables: fluxes, trajectories, GDU numbers and errors | TT_2000 | ns since J2000 |
| epoch_timetag | Time tags for optics state and GDU energies | TT_2000 | ns since J2000 |

| | | | |
|---|---|---|---|
| mms<N>_edi_optics_state_srvy_l2 | EDI detector optics state | UINT1 | none |
| mms<N>_edi_energy_gdu1_srvy_l2 | EDI GDU1 energy | UINT2 | eV |
| mms<N>_edi_energy_gdu2_srvy_l2 | EDI GDU2 energy | UINT2 | eV |
| mms<N>_edi_gdu_0_srvy_l2 | GDU number for pitch angle 0 data | UINT1 | none |
| mms<N>_edi_gdu_180_srvy_l2 | GDU number for pitch angle 180 data | UINT1 | none |
| mms<N>_edi_flux1_0_delta_srvy_l2 | Error for pitch angle 0 flux | FLOAT | $cm^{-2}\ s^{-1}$ |
| mms<N>_edi_flux1_180_delta_srvy_l2 | Error for pitch angle 180 flux | FLOAT | $cm^{-2}\ s^{-1}$ |

### 4.3.2 Burst

File Names:

mms<N>_edi_brst_l2_amb_<yyyymmddhhmmss>_v<x.y.z>.cdf
mms<N>_edi_brst_l2_amb-pm2_<yyyymmddhhmmss>_v<x.y.z>.cdf

| Name | Description | Type | Unit |
|---|---|---|---|
| mms<N>_edi_flux1_0_brst_l2<br>mms<N>_edi_flux2_0_brst_l2<br>mms<N>_edi_flux3_0_brst_l2<br>mms<N>_edi_flux4_0_brst_l2 | Electron flux in four separate directional channels close to pitch angle 0 | FLOAT | $cm^{-2}\ s^{-1}$ |
| mms<N>_edi_flux1_180_brst_l2<br>mms<N>_edi_flux2_180_brst_l2<br>mms<N>_edi_flux3_180_brst_l2<br>mms<N>_edi_flux4_180_brst_l2 | Electron flux in four separate directional channels close to pitch angle 180 | FLOAT | $cm^{-2}\ s^{-1}$ |
| mms<N>_edi_traj1_gse_0_brst_l2<br>mms<N>_edi_traj2_gse_0_brst_l2<br>mms<N>_edi_traj3_gse_0_brst_l2<br>mms<N>_edi_traj4_gse_0_brst_l2 | Particle motion directions for the four channels close to pitch angle 0 in GSE | FLOAT | degrees |
| mms<N>_edi_traj1_gse_180_brst_l2<br>mms<N>_edi_traj2_gse_180_brst_l2<br>mms<N>_edi_traj3_gse_180_brst_l2<br>mms<N>_edi_traj4_gse_180_brst_l2 | Particle motion directions for the four channels close to pitch angle 180 in GSE | FLOAT | degrees |
| mms<N>_edi_traj1_gsm_0_brst_l2<br>mms<N>_edi_traj2_gsm_0_brst_l2<br>mms<N>_edi_traj3_gsm_0_brst_l2<br>mms<N>_edi_traj4_gsm_0_brst_l2 | Particle motion directions for the four channels close to pitch angle 0 in GSM | FLOAT | degrees |
| mms<N>_edi_traj1_gsm_180_brst_l2<br>mms<N>_edi_traj2_gsm_180_brst_l2<br>mms<N>_edi_traj3_gsm_180_brst_l2<br>mms<N>_edi_traj4_gsm_180_brst_l2 | Particle motion directions for the four channels close to pitch angle 180 in GSM | FLOAT | degrees |
| **Support data** | | | |
| epoch_0 | Time tags for pitch angle 0 variables: fluxes, trajectories, GDU numbers and errors | TT_2000 | ns since J2000 |
| epoch_180 | Time tags for pitch angle 180 variables: fluxes, trajectories, GDU numbers and errors | TT_2000 | ns since J2000 |
| epoch_timetag | Time tags for optics state and | TT_2000 | ns since |

| | | | |
|---|---|---|---|
| | GDU energies | | J2000 |
| mms<N>_edi_optics_state_brst_l2 | EDI detector optics state | UINT1 | none |
| mms<N>_edi_energy_gdu1_brst_l2 | EDI GDU1 energy | UINT2 | eV |
| mms<N>_edi_energy_gdu2_brst_l2 | EDI GDU2 energy | UINT2 | eV |
| mms<N>_edi_gdu_0_brst_l2 | GDU number for pitch angle 0 data | UINT1 | none |
| mms<N>_edi_gdu_180_brst_l2 | GDU number for pitch angle 180 data | UINT1 | none |
| mms<N>_edi_flux1_0_delta_brst_l2<br>mms<N>_edi_flux2_0_delta_brst_l2<br>mms<N>_edi_flux3_0_delta_brst_l2<br>mms<N>_edi_flux4_0_delta_brst_l2 | Errors for pitch angle 0 flux channels | FLOAT | $cm^{-2}\ s^{-1}$ |
| mms<N>_edi_flux1_180_delta_brst_l2<br>mms<N>_edi_flux2_180_delta_brst_l2<br>mms<N>_edi_flux3_180_delta_brst_l2<br>mms<N>_edi_flux4_180_delta_brst_l2 | Errors for pitch angle 180 flux channels | FLOAT | $cm^{-2}\ s^{-1}$ |

## 4.4 Ambient Electron Calibration File

Filenames:

mms<N>_edi_cal_l2_amb_20150312_v<x.y.z>.cdf

| Name | Description | Type | Unit |
|---|---|---|---|
| mms<N>_edi_rel_gdu1_cal_l2 | GDU1 relative calibration factor as a function of polar angle and azimuth angle of the detector look direction | FLOAT | none |
| mms<N>_edi_rel_gdu2_cal_l2 | GDU1 relative calibration factor as a function of polar angle and azimuth angle of the detector look direction | FLOAT | none |
| mms<N>_edi_abs_gdu1_cal_l2 | GDU1 absolute calibration factor for conversion to fluxes | FLOAT | $cm^{-2}\ s^{-1}$ |
| mms<N>_edi_abs_gdu2_cal_l2 | GDU2 absolute calibration factor for conversion to fluxes | FLOAT | $cm^{-2}\ s^{-1}$ |
| **Support Variables** | | | |
| Epoch | Unused | | |
| mms<N>_edi_phi | Azimuth angle for each azimuthal look direction bin (sensor anode pad) | FLOAT | degrees |
| mms<N>_edi_theta | Polar angle for each polar look direction bin | FLOAT | degrees |
| epoch_rel | Time tags for relative calibration parameters | TT2000 | ns since J2000 |
| epoch_abs | Time tags for absolute calibration parameters | TT2000 | ns since J2000 |
| mms<N>_edi_optics_rel_cal_l2 | Optics state for relative calibration | FLOAT | none |
| mms<N>_edi_optics_abs_cal_l2 | Optics state for absolute calibration | UINT2 | none |

# 5 Quicklook Data Products

## 5.1 Survey Ambient Quicklook Data

| Name | Description | Type | Unit |
|---|---|---|---|
| mms<N>_edi_counts1_0 | Counts along pitch angle zero with dead time correction and relative calibration applied | UINT2 | counts |
| mms<N>_edi_counts1_180 | Counts along pitch angle 180 with dead time correction and relative calibration applied | UINT2 | counts |
| **Support Variables** | | | |
| Epoch | Unused | | |
| epoch_0 | Time tags for pitch angle 0 data | TT2000 | Ns since J2000 |
| epoch_180 | Time tags for pitch angle 180 data | TT2000 | Ns since J2000 |
| epoch_timetag | Time tags for optics state and energy variables | TT2000 | Ns since J2000 |
| mms<N>_edi_optics_state | Optics State | UINT1 | None |
| mms<N>_edi_energy_gdu1 | GDU1 detector energy | UINT2 | eV |
| mms<N>_edi_energy_gdu2 | GDU2 detector energy | UINT2 | eV |
| mms<N>_edi_gdu_0 | GDU number for pitch angle 0 data | UINT1 | None |
| mms<N>_edi_gdu_180 | GDU number for pitch angle 180 data | UINT1 | None |